Structural Study of the C2 Domains of the Classical PKC Isoenzymes Using Infrared Spectroscopy and Two-Dimensional Infrared Correlation Spectroscopy†

Alejandro Torrecillas, Senena Corbalán-García, and Juan C. Gómez-Fernández*

Departamento de Bioquímica y Biología Molecular (A), Facultad de Veterinaria, Universidad de Murcia, Apartado de Correos 4021, E-30080-Murcia, Spain

Received May 9, 2003; Revised Manuscript Received June 20, 2003

ABSTRACT: The secondary structure of the C2 domains of the classical PKC isoenzymes, α, βII, and γ, has been studied using infrared spectroscopy. Ca^{2+} and phospholipids were used as protein ligands to study their differential effects on the isoenzymes and their influence on thermal protein denaturation. Whereas the structures of the three isoenzymes were similar in the absence of Ca^{2+} and phospholipids at 25 °C, some differences were found upon heating in their presence, the C2 domain of the γ-isoenzyme being better preserved from thermal denaturation than the domain from the α-isoenzyme and this, in turn, being better than that from the β-isoenzyme. A two-dimensional correlation study of the denaturation of the three domains also showed differences between them. Synchronous 2D-IR correlation showed changes (increased aggregation of denaturated protein) occurring at 1616−19 cm^{-1}, and this was found in the three isoenzymes. On the other hand, the asynchronous 2D-IR correlation study of the domains in the absence of Ca^{2+} showed that, in all cases, the aggregation of denaturated protein increased after changes in other structural components, an increase perhaps related with the hard-core role of the β-sandwich in these proteins. The differences observed between the three C2 domains may be related with their physiological specialization and occurrence in different cell compartments and in different cells.

Protein kinase C (PKC) is a phospholipid-dependent serine/threonine kinase family consisting of at least 10 closely related isoenzymes (*1*, *2*). The different PKC isoenzymes play important roles in signal transduction pathways, although the exact significance of each isoenzyme is not fully understood at present.

There are three main classes of PKC isoenzymes: the classical (α, βI, βII, and γ), that contain the conserved C1 and C2 motifs in the regulatory domain and which are activated by both Ca^{2+}-dependent phospholipid binding and diacylglycerol; the novel (δ, ε, η, θ, and μ), which also contain C1 and C2 motifs, although located in reverse order from those of the classical isoenzymes, and which are activated by phospholipid and diacylglycerol binding in a Ca^{2+}-independent manner; and finally, the atypical isoenzymes (ζ and ι/λ), whose regulatory domain does not contain any conserved modules and which are not activated by either Ca^{2+} or diacylglycerol (*3*).

C2 domains are sequence motifs that contain approximately 130 amino acids and are present in a large variety of proteins involved in intracellular signaling and membrane trafficking. High-resolution structures of C2 domains from synaptotagmin (*4*−*6*), phospholipase C-δ (*7*, *8*), phospholipase A2 (*9*−*11*), PKCβI (*12*), PKCδ (*13*), PKCα (*14*, *15*), PKCε (*16*), PTEN (*17*), and PI3K (*18*) have revealed a highly homologous β-sandwich tertiary fold which, in the first four proteins, serves as the scaffold for a bipartite Ca^{2+} binding site that is formed by a pair of loops projecting from the opposing β-sheets. The C2 domains of synaptotagmin and the two phospholipases, respectively, adopt type I and type II connectivities that differ only in the circular permutation of the N and C termini with respect to the tertiary fold (reviewed in *19* and *20*). The C2 domains of classical PKCs can be classified as having a type I topology (*12*, *14*, *15*). Novel PKCs (PKCδ), on the other hand, exhibit a type II topology similar to that of the phospholipases, although the Ca^{2+} binding site is degenerated (*13*, *16*).

In the C2 domains that bind Ca^{2+}, as in the case of those found in classical PKC isoenzymes, the residues that define the calcium binding sites form part of the loops on one side of the domain (*12*, *14*). Two or three Ca^{2+} ions have been found in the crystal structures of the C2 domains of both PKCβ (*12*) and PKCα (*14*, *15*). In turn, anionic phospholipids have been shown to bind to the C2 domain of PKCα in two different locations, namely in the Ca^{2+} binding pocket and in the vicinity of the lysine-rich cluster at strands β3 and β4 (*15*).

It is known that the Ca^{2+}-dependent binding of PKC to membranes requires anionic lipids (*21*, *22*). In the absence of diacylglycerol, Ca^{2+} increases the affinity of PKC for anionic phospholipids, which only require a negative charge (*23*). It has been demonstrated both in vivo and in vitro that the C2 domain of PKCα mediates in this Ca^{2+}-dependent binding (*24*, *25*).

† This work was supported by Grants BMC2002-00119 from Dirección General de Investigación, Ministerio de Ciencia y Tecnología (Spain), and PI-35/00789/FS/01 from Fundación Séneca (Comunidad Autónoma de Murcia, Spain). A.T. is a recipient of a fellowship from Fundación Séneca (Murcia, Spain). S.C.-G. belongs to "Ramón y Cajal Program" supported by Ministerio de Ciencia y Tecnología y Universidad de Murcia.

* Corresponding author. Telephone: +34-968-364766. Fax: +34-968-364766. E-mail: jcgomez@um.es.

10.1021/bi034759+ CCC: $25.00
Published on Web 09/23/2003

```
                  β1                  β2          CBR1        β3
C2α   157  EKR GRIYLKAEV-T D  EKLHVTVRDAK NLIPMDPNGLS DPYVKLKLI PDPKNESK
C2βII 157  ERR GRIYIQAHI-D R  EVLIVVVRDAK NLVPMDPNGLS DPYVKLKLI PDPKSESK
C2γ   157  ERR GRLQLEIRAPTSD  E-IHITVGEAR NLIPMDPNGLS DPYVKLKLI PDPRNLTK

          β4   CBR2      β5                    β6      CBR3    β7
C2α   210 QKT KTIRSTLN PQWNESFTFKL KPSDKD RRLSVEIWDW DRTTAN DFMGSLSFGV
C2βII 210 QKT KTIKCSLN PEWNETFRFQL KESDKD RRLSVEIWDW DLTSRN DFMGSLSFGI
C2γ   210 QKT KTVKATLN PVWNETFVFNL KPGDVE RRLSVEVWDW DRTSRN DFMGAMSFGV

          α1      β8      α2
C2α   264 SELMK MP ASGWYKL LN QEEG EYYNVPIPEG     293
C2βII 264 SELQK AG VDGWFKL LS QEEG EYFNVPVPPEG    294
C2γ   264 SELLK AP VDGWYKL LN QEEG EYYNVPVADADNCS 297
```

FIGURE 1: Primary amino sequence alignment for the isolated C2 domains of PKCα, PKC*β*II, and PKC*γ*. Calcium binding regions (CBR) and *β*-sheets are assigned according to the designations of the C2 domains of the PKCα (*14*, *15*) and PKC*β*I (*12*) crystal structures. The yellow boxes indicate identical residues. Homologous residues are colored in blue. The coordinating-calcium residues of the C2 domains of PKCα and PKC*β*I crystal structures are colored in red.

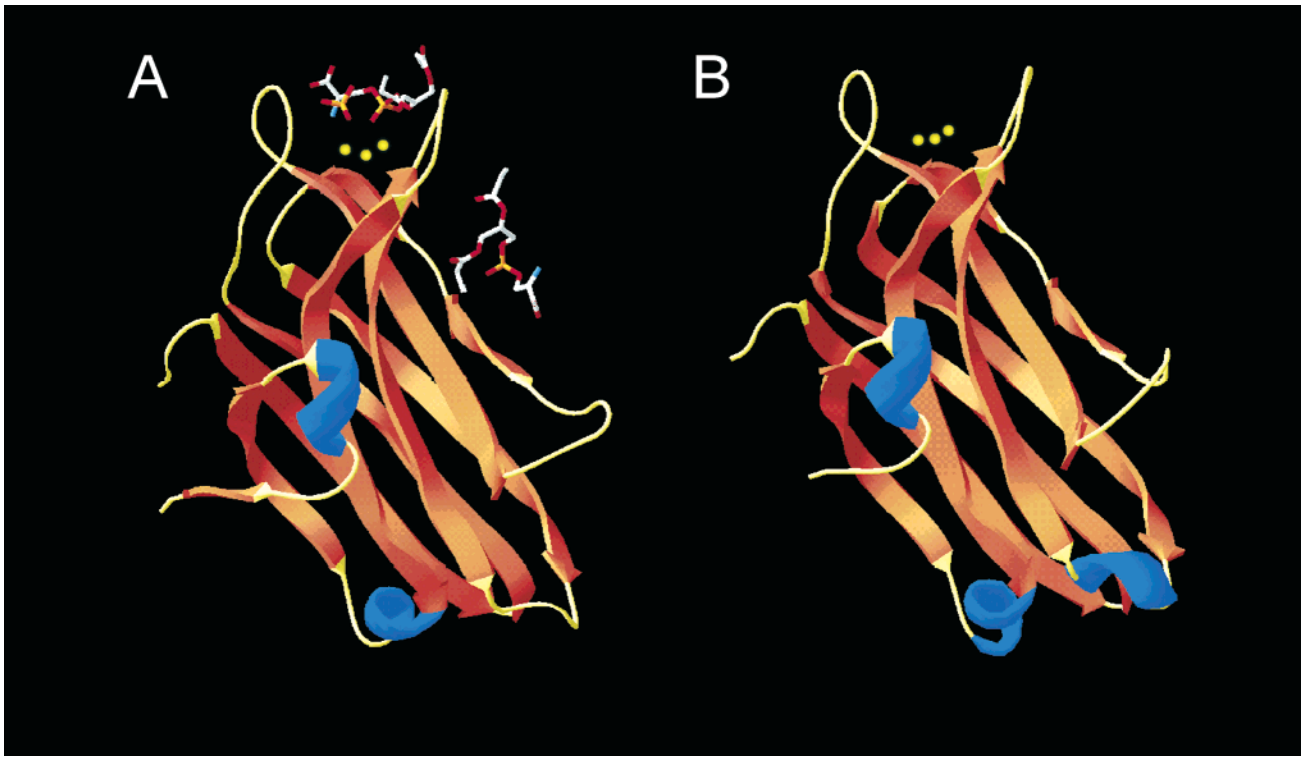

FIGURE 2: Available X-ray structures: (A) PKCα (*15*) and (B) PKC*β*I (*12*) isolated C2 domains. The PKCα-C2 domain was cocrystallized in the presence of calcium and the short-chain lipid 1,2-diacetyl-*sn*-phosphatidyl-L-serine (DAPS). Calcium ions are shown in yellow. The phosphate group and phospholipd molecules are depicted as filled sticks.

We will focus our attention in this paper on the classical PKCs (namely α, *β*II, and *γ*) which have similar structural and enzymatic properties but which are distributed in tissues and cells in a type-specific manner (see for reviews, *26*, *27*), with different levels of expression. Hence, PKCα is found in all cell types, PKC*β*I and PKC*β*II are found in several tissues, while PKC*γ* is found only in the central nervous system (*28*).

Figure 1 shows that the primary amino acid sequences of the different isoenzymes that belong to this group of classical PKCs are 64% identical. The same gene codifies both *β*I and *β*II isoenzymes, which differ in only the 50 aminoacyl residues of their extreme C-terminal ends (*29*). The 3D structures of the C2 domains from PKCα and PKC*β*I are also very similar with just a 0.43 Å rms deviation between the equivalent C_α atoms (Figure 2). However, since, as has been commented above, there seems to be a degree of specialization with respect to the function of these isoenzymes and since they function in very different cells and compartments, some structural specificities might be expected from the fact that they are activated by different Ca^{2+} concentrations and biomembranes with different lipid compositions. Although no structural information is available for PKC*γ*, the high sequence identity indicates that the PKC*γ*-

C2 domain possesses a structure similar to that of the C2 domains from other conventional PKCs. In particular, the PKCγ-C2 domain is 74% and 69% identical to the PKCα-C2 and PKCβ-C2 domains, respectively (*30*−*32*).

In the present work we have used infrared spectroscopy and two-dimensional infrared correlation spectroscopy to investigate the structural differences existing between the different classical PKC isoenzymes. Infrared spectroscopy is a very well suited technique to study the secondary structure of proteins (*33*). Two-dimensional infrared (2D-IR) correlation spectroscopy (*34*−*36*) is a modern technique with a very broad potential in the study of proteins. This technique has four main advantages: (i) The 2D-IR correlation spectroscopy deconvolutes amide bands into component bands due to different secondary structures. (ii) It allows the establishment of correlations between bands due to different secondary structures of protein through selective correlation peaks for a given conformation. (iii) It enables us to monitor intensity variations even in very weak protein bands. (iv) It provides information about the specific order of secondary structural changes and changes under various environments (*36*).

We demonstrate in this paper that some significant differences exist in their secondary structures and that these differences probably form the basis of their different interactions with Ca^{2+} and phospholipids. In addition, their different susceptibilities to thermal denaturation may reflect different backbone motions of the three isoforms, this being potentially very interesting to understand their different functionalities.

MATERIALS AND METHODS

Materials. 1-Palmitoyl-2-oleoyl-*sn*-glycero-3-phosphocholine (POPC) and 1-palmitoyl-2-oleoyl-*sn*-glycero-3-phosphate (POPA) were purchased from Avanti Polar Lipids, Inc. (Alabaster, AL). 1,2-Dipalmitoyl-L-3-phosphatidyl[*N*-methyl-^3H]choline was purchased from Dupont (Boston, MA). Isopropyl 1-thio-β-D-galactopyranoside (IPTG) was purchased from Roche Diagnostics (Barcelona, Spain). Ni−NTA agarose was purchased from QUIAGEN (Hilden, Germany), and Glutathione-Sepharose beads were purchased from Amersham Pharmacia Biotech AB (Uppsala, Sweden). Sephadex G-100 was purchased form Sigma (Madrid, Spain). Deuterated water (deuterium oxide) was purchased from Aldrich Chemical Co. (Madrid, Spain). Water was twice distilled and deionized using a Millipore system from Millipore Ibérica (Madrid, Spain).

Preparation of Phospholipids. Lipid vesicles were generated by mixing chloroform solutions of 1-palmitoyl-2-oleoyl-*sn*-glycero-3-phosphocholine (POPC) and 1-palmitoyl-2-oleoyl-*sn*-glycero-3-phosphate (POPA) at the desired proportions (POPC/POPA, molar ratio 1:4). Lipids were dried from the organic solvent under a stream of oxygen-free nitrogen, and then the last traces of organic solvent were removed under vacuum for at least 2 h. 1,2-Dipalmitoyl-L-3-phosphatidyl-[*N*-methyl-^3H]choline ([^3H]DPPC, specific activity of 56 Ci/mmol) was included in the lipid mixture for the gel filtration assays as a tracer, at a concentration of approximately 3000−6000 cpm/mg of phospholipid. Dried phospholipids were resuspended in the corresponding buffers by vigorous vortexing and subjected to direct probe sonication (10 cycles of 15 s) to produce small unilamellar vesicles (SUVs). These buffers were 25 mM Hepes pH 7.4, 100 mM NaCl, 0.2 mM EGTA for the PKCα-C2 domain, 20 mM MOPS pH 6.8, 100 mM NaCl, 0.2 mM EGTA for the PKCβII-C2 domain, and 25 mM Tris-HCl pH 8, 100 mM NaCl, 0.2 mM EGTA for the PKCγ-C2 domain.

Construction of the Expression Plasmids. PKCα and PKCβII were kind gifts from Drs. Nishizuka and Ono (Kobe University, Kobe, Japan), and PKCγ cDNA was a kind gift from Dr. Tobias Meyer (Stanford University Medical School, Stanford, CA). The DNA fragments corresponding to the C2 domains of PKCβII (residues 157−295) and PKCγ (residues 156−298) were amplified using PCR with oligonucleotides βEco5 and βHind3 (sequences 5′-AAGGAATTCACACAGAACGCCGT-3′ and 5′-AATAAGCTTTCATCCTTCCGG CGG-3′) and γEco5 and γHind3 (sequences 5′-AAGGAATTCATACAGAGCGCCGTG-3′ and 5′-ACCAAGCTTTCAGCTGCAGTTGTC-3′), respectively. The resulting 417 bp and 429 bp PCR fragments were subcloned into the EcoRI and HindIII sites of the bacterial expression vector pET28c(+), in which the inserts are fused to a six-histidine tag. All constructs were confirmed by DNA sequencing. The C2 domain of PKCα was obtained as previously described (*37*).

Expression and Purification of the His-PKC-C2 Domains. The pET28c(+) plasmid containing PKC-C2 domains were transformed into BL21 (DE3) *Escherichia coli* cells. The bacterial cultures (OD_{600} = 0.6) were induced for 5 h at 30 °C with 0.5 mM isopropyl 1-thio-β-D-galactopyranoside (IPTG). The cells were lysed by sonication in lysis buffer containing protease inhibitors (10 mM benzamidine, 1 mM PMSF, and 10 $\mu g \cdot mL^{-1}$ trypsin inhibitor). The lysis buffers for PKCα, PKCβII, and PKCγ C2 domains contained 25 mM Hepes pH 7.4 and 100 mM NaCl, 20 mM MOPS pH 6.8 and 100 mM NaCl, and 25 mM Tris-HCl pH 8 and 100 mM NaCl, respectively. The soluble fraction of the lysate was incubated with Ni−NTA agarose for 2 h at 4 °C. The Ni beads were washed with lysis buffer containing 20 mM imidazole. The bound proteins were eluted with the same buffer containing 50, 250, and 500 mM imidazole. The six-histidine tag was removed after thrombin cleavage, and finally, the PKC-C2 domain was washed with the same buffer and concentrated using an Ultrafree-5 centrifugal filter unit (Millipore Inc, Bedford, MA). Protein concentrations were determined using the method described by Smith et al. (*38*). The purity of the samples was checked by means of a 15% SDS−polyacrylamide gel electrophoresis and Coomassie Blue (Sigma, St. Louis, MO) staining.

Gel Filtration Assay. This assay was carried out as described by García-García et al. (*33*). Samples containing 80 μg of the PKC-C2 domain and 400 μg of small unilamellar vesicles (POPC/POPA, molar ratio 1:4) labeled with [^{3}H]DPPC were incubated in 100 μL of the corresponding buffer for 10 min. These buffers were 25 mM Hepes pH 7.4, 100 mM NaCl, 0.2 mM $CaCl_2$ for the PKCα-C2 domain, 20 mM MOPS pH 6.8, 100 mM NaCl, 0.2 mM $CaCl_2$ for the PKCβII-C2 domain, and 25 mM Tris-HCl pH 8.0, 100 mM NaCl, 0.2 mM $CaCl_2$ for the PKCγ-C2 domain. Note that this molar ratio (protein/lipids/calcium) was the same as that used in the FTIR assays. The sample was applied on a Sephadex G-100 column (1.0 cm × 2.5 cm) equilibrated and eluted with the same buffers. Fractions of 100 μL were collected. The phospholipid elution profile was determined

by measuring the radioactivity contained in each fraction by liquid scintillation. The PKC-C2 domain elution profile was determined by densitometry after using a 15% SDS−polyacrylamide gel and silver staining of each fraction. A control assay was carried out without phospholipids. SDS−polyacrylamide gel electrophoresis was carried out according to Laemmli (*39*) with a 5% stacking and a 15% separating gel. Proteins were detected by silver staining (Bio-Rad, Richmond, CA).

IR Spectroscopy. C2 domains from PKCα, PKCβII, and PKCγ were prepared at 8 mg·mL^{-1} in D_2O buffers. These buffers were 25 mM Hepes pD 7.4, 100 mM NaCl, 0.2 mM EGTA for the PKCα-C2 domain, 20 mM MOPS pD 6.8, 100 mM NaCl, 0.2 mM EGTA for the PKCβII-C2 domain, and 25 mM Tris-HCl pD 8, 100 mM NaCl, 0.2 mM EGTA for the PKCγ-C2 domain.

The proteins were incubated overnight at 4 °C to maximize H−D exchange. To study the infrared amide bands of the proteins in the presence of lipids, small unilamellar vesicles in the corresponding D_2O buffers were mixed with the protein solutions. The lipid mixtures contained POPC/POPA (molar ratio 1:4) and were prepared at 40 mg·mL^{-1}.

Infrared spectra were recorded using a Bruker Vector 22 Fourier transform infrared spectrometer equipped with a MCT detector. Samples were examined in a thermostated Specac 20 710 cell (Specac, Kent, U.K.) equipped with CaF_2 windows and 25 μm spacers. The spectra were recorded after equilibrating the samples at 20 °C for 20 min in the infrared cell. A total of 128 scans were accomplished for each spectrum with a nominal resolution of 2 cm^{-1} and then Fourier transformed using a triangular apodization function. A sample shuttle accessory was used to obtain the average background and sample spectra. The sample chamber of the spectrometer was continuously purged with dry air to prevent atmospheric water vapor from obscuring the bands of interest. Samples were scanned between 20 and 80 °C at 5 °C intervals with a 5 min delay between each scan using a circulation water bath interfaced to the spectrometer computer. Spectral subtraction was performed interactively using the Grams/32 program (Galactic Industries Corporation, Salem, NH). The spectra were subjected to deconvolution and second-derivation using the same software. Fourier self-deconvolution was carried out using a Bessel smoothing function, a Lorentzian shape with a γ factor of 10, and a full width at half-heigth of 20 cm^{-1}. Both deconvolution and derivation gave the number and position, as well as an estimation of the bandwidth and the intensity of the bands making up the amide I region. Thereafter, curve fitting was performed and the heights, widths, and positions of each band were optimized successively. Data treatment and band decomposition of the original amide I have been described previously (*40*, *41*). The fractional areas of the bands in the amide I region were calculated from the final fitted band areas.

Two-dimensional correlation analysis was carried out using the 2D-Pocha program written by D. Adachi and Y. Ozaki (Kwansei Gakuin University, Japan) obtained from the website http://science.kwansei.ac.jp/~ozaki/2D-Pocha.htm. This software can calculate the two-dimensional correlation spectroscopy proposed by I. Noda (*34*). The maximum intensity of the whole correlation map is divide by 6, giving place to a contour map in which the main peak, that is, the one with the maximum intensity, will be surrounded by six contour lines and the rest of the peaks will show a number of contour lines which will reflect their intensities in relation to the main peak.

To obtain the 2D-IR maps, heating was used as the perturbation to induce time-dependent spectral fluctuations and to detect dynamical spectral variations of the secondary structure of the C2 domains. The mathematical background for generalized 2D correlation spectroscopy has been described in detail (*34*). The following procedures were taken to obtain a generalized 2D correlation of temperature-dependent infrared spectra. Given an infrared spectral intensity variation $A(\nu, T)$ observed in a temperature range between T_{min} and T_{max}, the synchronous and asynchronous 2D-IR correlation intensities $\Phi(\nu_1, \nu_2)$ and $\Psi(\nu_1, \nu_2)$ become

$$\Phi(\nu_1, \nu_2) + i\Psi(\nu_1, \nu_2) = \frac{1}{\pi(T_{max} - T_{min})}\int_0^\infty Y_1(\omega)\, Y_2^*(\omega)\, d\omega$$

where $Y_1(\omega)$ is the temperature domain Fourier transform of $A(\nu_1, \nu_2)$ and $Y^*_2(\omega)$ is the conjugate of the Fourier transform of $A(\nu_2, T)$.

As reviewed by Noda (*34*), the synchronous 2D correlation spectrum of dynamic spectral intensity variations represents the simultaneous coincidental changes of spectral intensities measured at ν_1 and ν_2. Correlation peaks appear at both diagonal (autopeaks) and off-diagonal peaks (cross-peaks). The asynchronous spectrum of dynamic spectral intensity variations represents sequential, or unsynchronized, changes of spectral intensities measured at ν_1 and ν_2. The asynchronous spectrum has no autopeaks, consisting exclusively of cross-peaks located at off-diagonal positions. An asynchronous cross-peak develops only if the intensities of two dynamic spectral intensities vary out of phase with each other for some Fourier-frequency components of signal fluctuations.

RESULTS

The secondary structures of classic PKC isoenzymes, PKCα, PKCβII, and PKCγ, were studied by using infrared spectroscopy. The amide I′ band decomposition of the native PKCα-C2 domain in D_2O and 0.2 mM EGTA at 25 °C is shown in Figure 3A. The number and initial position of the component bands were obtained from band-narrowed spectra by Fourier deconvolution and derivation (Figure 3C). The corresponding parameters, that is, band position and percentage area of each spectral component and assignment, are shown in Table 1. The spectra in D_2O exhibit seven component bands in the 1700−1600 cm^{-1} region, and the quantitative contribution of each band to the total amide I′ contour was obtained by band curve-fitting of the original spectra. The major component in the amide I′ region appears at 1634 cm^{-1} and so clearly arises from intramolecular C═O vibrations of the β-sheets (*40*−*46*). The high-frequency component at 1676 cm^{-1} can be assigned to the antiparallel β-sheet structure (*40*, *47*). The 1654 cm^{-1} component is usually assigned to the α-helix (*41*, *42*, *48*). The band near 1644 cm^{-1} can be attributed to nonstructured conformations (*44*, *49*). The bands located at 1663 and 1688 cm^{-1} arise from β-turns (*40*, *47*). Additionally, there is a band at about

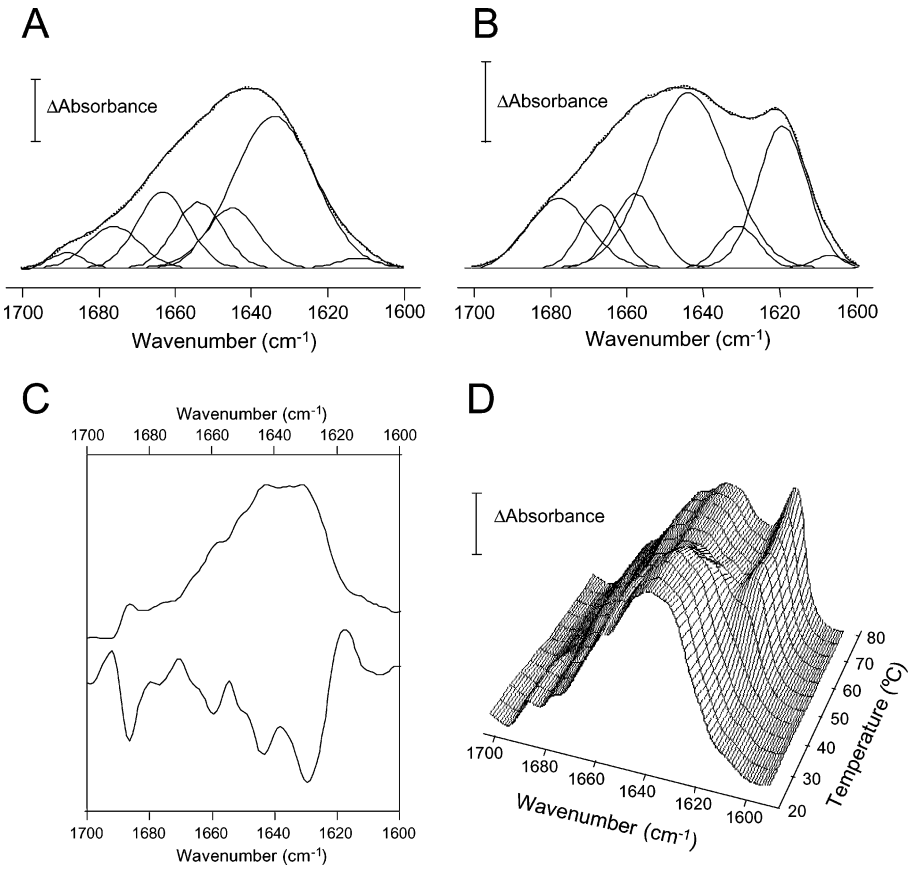

FIGURE 3: FT-IR spectra (solid line) of the PKCα-C2 domain in the amide I′ region at 25 °C (A) and 80 °C (B) in D_2O buffer in the absence of calcium with the fitted component bands. The parameters corresponding to the component bands are shown in Table 1. The dashed line represents the curve-fitted spectrum. (C) Deconvolved (upper trace) and second-derivated (bottom trace) spectra of the PKCα-C2 domain in the amide I′ region at 25 °C. (D) Deconvolved FT-IR spectra of the PKCα-C2 domain in the amide I′ region (1700−1600 cm^{-1}) as a function of temperature, from 25 to 80 °C. The protein concentration was approximately 8 mg·mL^{-1}. The increment of absorbance units (ΔAbs) was 0.02.

Table 1: FT-IR Parameters of the Amide I′ Band Components of the Classical PKCα, βII, and γ C2 Domains in the Corresponding D_2O Buffers with 0.2 mM EGTA

	25 °C						80 °C					
	C2-PKCα domain		C2-PKCβII domain		C2-PKCγ domain		C2-PKCα domain		C2-PKCβII domain		C2-PKCγ domain	
assignment	position[a] (cm^{-1})	area[b] (%)	position (cm^{-1})	area (%)	position (cm^{-1})	area (%)	position (cm^{-1})	area (%)	position (cm^{-1})	area (%)	position (cm^{-1})	area (%)
β-turns	1688	2	1687	2	1688	2						
aggregated β-sheet							1679	13	1679	10	1679	11
antiparallel β-sheet	1676	9	1675	8	1674	8						
β-turns	1663	15	1662	14	1663	13	1667	8	1667	9	1667	9
α-helix	1654	12	1653	13	1653	14	1657	10	1657	11	1657	11
random	1644	12	1644	13	1644	13	1644	42	1643	37	1644	37
β-sheet	1634	50	1632	50	1632	50	1630	5	1630	9	1631	11
aggregated β-sheet							1619	22	1619	24	1619	21

[a] Peak position of the amide I′ band components. [b] Percentage area of the amide I′ band components. The area corresponding to side chain contributions located at 1615−1600 cm^{-1} has not been considered.

1610 cm^{-1}, which has been assigned to side chain absorption (*48*−*50*), and therefore its contribution is not included in the calculation of the secondary structure of PKC-C2. The secondary structure of the PKCα-C2 domain obtained from Table 1 is 59% β-sheet (taking into account the 1634 and 1676 cm^{-1} bands), 12% α-helix, 17% β-turns, and 12% nonstructured conformation. Very similar results were obtained for the secondary structure of the PKCβII-C2 and PKCγ-C2, as seen in Table 1, with differences of only 1−2% in some components, which are within experimental error. The procedure used here to quantitatively calculate the secondary structure is usually assumed to have an error of about 1% (*41*), and in this paper we have assumed it to be 1−2% as deduced from the comparison of at least three independent experiments and the repetition of the fitting procedure by three different persons; therefore, we will estimate as being significantly different, changes in the structural components of 4% or higher.

We studied the effect of Ca^{2+} binding on the secondary structure of the PKCα-C2 domains using 2 and 12 mM $CaCl_2$, which, under the conditions of the assay, represent Ca^{2+}/protein ratios of approximately 4:1 and 24:1, respec-

Table 2: FT-IR Parameters of the Amide I′ Band Components of the Classical PKCα, βII, and γ C2 Domains in the Corresponding D_2O Buffers in the Presence of 2 mM Ca^{2+}

	25 °C						80 °C					
	C2-PKCα domain		C2-PKCβII domain		C2-PKCγ domain		C2-PKCα domain		C2-PKCβII domain		C2-PKCγ domain	
assignment	position[a] (cm^{-1})	area[b] (%)	position (cm^{-1})	area (%)	position (cm^{-1})	area (%)	position (cm^{-1})	area (%)	position (cm^{-1})	area (%)	position (cm^{-1})	area (%)
β-turns	1688	3	1687	2	1688	3						
aggregated β-sheet							1679	14	1679	10	1679	13
antiparallel β-sheet	1675	9	1676	7	1676	9						
β-turns	1662	15	1663	14	1664	14	1666	9	1667	8	1667	10
α-helix	1654	12	1654	14	1655	14	1657	10	1657	10	1657	13
random	1644	12	1644	13	1645	12	1644	39	1643	38	1645	34
β-sheet	1635	49	1634	50	1633	48	1632	9	1630	10	1631	18
aggregated β-sheet							1620	19	1619	24	1619	12

Table 3: FT-IR Parameters of the Amide I′ Band Components of the Classical PKCα, βII, and γ C2 Domains in the Corresponding D_2O Buffers in the Presence of 12 mM Ca^{2+}

	25 °C						80 °C					
	C2-PKCα domain		C2-PKCβII domain		C2-PKCγ domain		C2-PKCα domain		C2-PKCβII domain		C2-PKCγ domain	
assignment	position[a] (cm^{-1})	area[b] (%)	position (cm^{-1})	area (%)	position (cm^{-1})	area (%)	position (cm^{-1})	area (%)	position (cm^{-1})	area (%)	position (cm^{-1})	area (%)
β-turns	1688	3	1687	2	1686	3					1688	2
aggregated β-sheet							1679	13	1679	10		
antiparallel β-sheet	1676	9	1676	8	1674	8					1676	8
β-turns	1663	15	1663	15	1662	14	1666	9	1667	8	1664	15
α-helix	1655	12	1654	14	1653	14	1657	10	1657	12	1655	14
random	1644	11	1645	12	1644	14	1644	35	1644	39	1645	14
β-sheet	1634	50	1634	49	1631	47	1631	16	1630	12	1633	47
aggregated β-sheet							1618	17	1619	19		

tively. While 2 mM is a nonsaturating concentration under the conditions of the FT-IR experiment, 12 mM is fully saturating. The spectra of PKCα-C2, PKCβII-C2, and PKCγ-C2 at 25 °C in the presence of 2 and 12 mM $CaCl_2$ were all very similar to those described above for the protein in the absence of $CaCl_2$ (not shown), including the number and position of the amide I′ component bands indicated in Tables 2 and 3.

To ascertain whether subtle structural changes occur during Ca^{2+} binding, thermal stability studies were carried out and important unfolding changes were observed in this process. In the case of PKCα-C2 in the absence of Ca^{2+} (Figure 3B), these changes included a broadening of the overall amide I′ contour and the appearance of well-defined components at 1619 and 1679 cm^{-1}, which are highly characteristic of thermally denatured proteins (*40*−*51*). These components indicate that extended structures were formed by aggregation of the unfolded proteins produced as a consequence of irreversible thermal denaturation (*41*, *51*, *52*). The 3D stacking of spectra (Figure 3C) clearly shows the profile change that takes place upon heating. Apart from the appearance of the 1618 and 1679 cm^{-1} components, other changes in the structure as a result of protein denaturation are of note (Table 1). The spectrum corresponding to 80 °C showed a 1644 cm^{-1} band as the major component, which corresponds to an unordered structure and represents 42% of the total area (Table 1). The band at 1630 cm^{-1} corresponds to a β-sheet structure and shows two main changes: the percentage of the total area decreased to 5%, and the maximum wavelength of this component shifted from 1634 cm^{-1} at 25 °C to 1630 cm^{-1} at 80 °C (Figure 3B). In addition, β-turn components appeared at 1667 cm^{-1} (12% in total), indicating that a part of this type of structure remains after denaturation, as has been seen in other cases (*41*). However, it is very interesting to note that the α-helix component appearing at 1654−1657 cm^{-1} was maintained after heating. Thus, it seems that thermal denaturation of the PKCα-C2 domain is characterized by irreversible aggregation and unfolding of the β-sheet structure into a more disordered structure that mainly consists of aggregated structures or edge β-sheets appearing at 1619 and 1679 cm^{-1}. Similar results were obtained with the other two C2 domains, although certain peculiarities existed, the main one being, in the case of PKCβII-C2 and PKCγ-C2, a smaller increase in the 1643 cm^{-1} component at 80 °C (amounting to 37% for both of them compared with 42% in PKCα-C2), accompanied by a more conserved β-sheet component at 1630−1631 cm^{-1} (which amounted to 9% and 11%, respectively, compared with 5% in the case of the α-isoenzyme).

In another set of experiments, the effects of nonsaturating (2 mM) and saturating (12 mM) Ca^{2+} on the thermal denaturation of the cPKC-C2 domains were studied. When looking into the effect of Ca^{2+} on the changes in composition induced by thermal denaturation at 80 °C, it was observed that in the cases of PKCα-C2 and PKCβ-C2 the presence of 2 mM Ca^{2+} (Table 2) did not produced any significative changes. The γ-isoenzyme appeared to be more sensitive to the presence of 2 mM Ca^{2+} (Table 2), with the 1619 cm^{-1} component increasing to only 12% (compare with 19% in the α-isoenzyme and 24% in the β-isoenzyme). Moreover, the γ-isozyme kept 18% of the β-sheet component (1631 cm^{-1}), and the random component (1645 cm^{-1}) increased

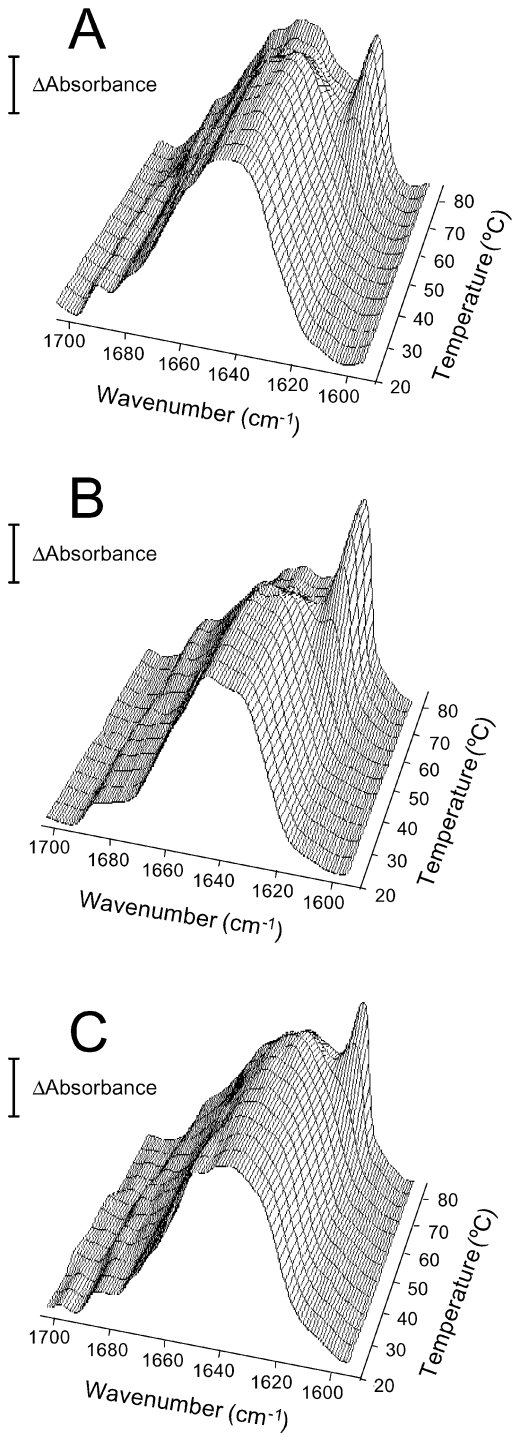

FIGURE 4: Deconvolved FT-IR spectra of the C2 domains of (A) PKCα, (B) PKCβII, and (C) PKCγ in the amide I′ region (1700−1600 cm^{-1}) as a function of temperature, from 25 to 80 °C. The protein concentration was approximately 8 mg·mL^{-1}. The increment of absorbance units (ΔAbs) was 0.02.

to only 34%. This is further illustrated by 3D-stacking of the spectra (Figure 4), where the three isoenzymes are compared in the presence of 2 mM Ca^{2+}, and in which it can be seen how the 1619 cm^{-1} component appeared at 60 °C in the case of the PKCα-C2 (Figure 4A), at 55 °C in the PKCβII-C2 (Figure 4B), and at 70 °C in the PKCγ-C2 (Figure 4C).

The protective effect of Ca^{2+} was even more clearly seen when the experiments were carried out in the presence of 12 mM Ca^{2+}. In this case, the component appearing at 1619 cm^{-1} for PKCα-C2 (Table 3) represented 17% of the total (22% in the absence of Ca^{2+}), and the random component (1644 cm^{-1}) was only 35% (42% without Ca^{2+}), while the β-sheet (1630 cm^{-1}) remained at 16%. In the case of the PKCβII-C2 (Table 3), the component at 1618 cm^{-1} amounted to 19% (24% in the absence of Ca^{2+}), with a modest increase in the β-sheet up to 12% (9% in the absence of Ca^{1-}). A much bigger effect was observed in the case of PKCγ-C2 (Table 3), since the component at 1619 cm^{-1} formed by the heating in the absence of Ca^{2+} did not appear at all, suggesting that Ca^{2+} protects most efficiently in this case. This is confirmed by the other components in this spectrum, which remain very similar in frequency and percentage to those found for the same sample at 25 °C.

Another set of experiments was directed at investigating the effect of 2 mM Ca^{2+} plus phospholipid vesicles, containing phosphatidic acid/phosphatidylcholine (PA/PC) in a 4:1 molar ratio. Although phosphatidylserine has been described as producing the maximum activation of classical PKCs, it was not thought appropriate to use this phospholipid in this experiment, since it could have absorbed infrared radiation in the region where the amide I′ band also absorbs, thereby generating interferences. To check whether the C2 domains were bound to the lipid mixture under the experimental conditions used in the FT-IR measurements, gel filtration assays were carried out as previously described (*37*). These experiments proved that all the C2 domains were bound to lipids under these conditions (data not shown). In the case of the PKCα-C2 spectrum, some important changes were observed at 25 °C compared with the sample in the presence of only 2 mM Ca^{2+} but in the absence of phospholipid. The most striking effect (Figure 5A and Table 4) was the reduction of the β-sheet component (at 1633 cm^{-1}) that decreased to 36%, compared with 48% in the absence of phospholipid. This was accompanied by an increase in the random (+11%) and α-helix components (+6%). Similar results were also found for the other two isoenzymes (Table 4). Heating in the presence of 2 mM Ca^{2+} and PA/PC vesicles (4:1 molar ratio) also produced interesting results compared with those obtained by heating in the presence of just 2 mM Ca^{2+} without phospholipid. Hence, in the case of PKCα-C2 at 80 °C (Figure 5B and Table 4), it was noticed that the presence of the phospholipid vesicles substantially protected the protein from denaturation. The most noteworthy effect was that the α-helix (1656 cm^{-1}) remained at 16% (18% at 25 °C), in contrast with the situation in the absence of phospholipid vesicles, in which this component fell to only 10%. Also of importance was the increase in β-turns (1692 and 1666 cm^{-1}) to 23% compared with the 16% obtained at 25 °C (1690 and 1664 cm^{-1}) and 9% in the presence of 2 mM Ca^{2+} but in the absence of phospholipid vesicles (1666 cm^{-1}). On the other hand, the component at 1618−1620 cm^{-1}, attributed to the aggregated β-sheet, only reached 6%, compared with 19% in the sample heated at 80 °C in the presence of 2 mM Ca^{2+} but in the absence of phospholipid vesicles (compare Tables 2 and 4). Besides, the random component (1644−1645 cm^{-1}) reached only 29%, compared with 39% in the absence of phospholipid vesicles. There was also a very considerable decrease in the β-sheet component (1631−1632 cm^{-1}) from 36% at 25 °C to a mere 13% at 80 °C, although this decrease was less than that observed in the absence of phospholipid, when it

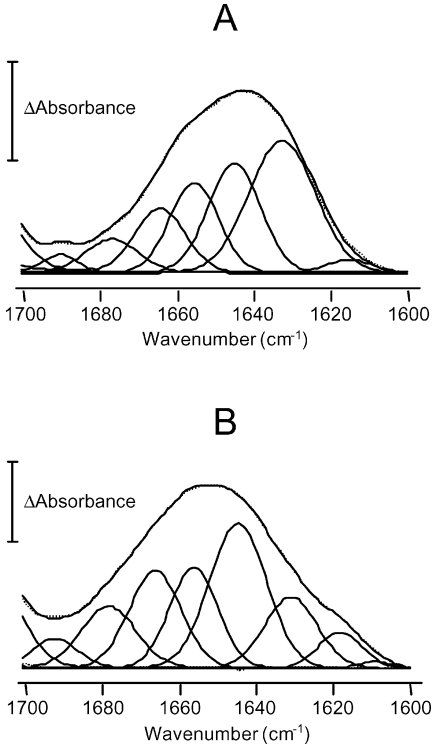

FIGURE 5: FT-IR spectra (solid line) with the fitted component bands of the PKCα-C2 domain in the amide I′ region at 25 °C (A) and 80 °C (B) in D_2O buffer in the presence of 2 mM Ca^{2+} and small unilamellar vesicles containing 20 mol % PC and 80 mol % PA. The parameters corresponding to the component bands are shown in Table 4. The dashed line represents the curve-fitted spectrum. The protein concentration was approximately 8 mg·mL^{-1}. The lipid final concentration was approximately 20 mg·mL^{-1}. The increment of absorbance units (ΔAbs) was 0.02.

was 9% at 80 °C. The same trend was observed for the PKCβII-C2 (Table 4), although in this case the random component (1645 cm^{-1}) increased up to 36% (29% in the α-isoenzyme) and the intermolecular β-sheet (1619 cm^{-1}) increased to 11% (compared with 7% in the α-isozyme). In addition, the 1680 cm^{-1} component, also associated with aggregation, only reached 7%, whereas in the α-isoenzyme it was 13%. In the case of the thermal denaturation of PKCγ-C2 in the presence of 2 mM Ca^{2+} and phospholipid vesicles (Table 4), the results produced were also similar to those for the PKCα-C2, although the β-sheet component (1631 cm^{-1}) remained at 19%, whereas the bands signaling aggregation went down, the 1679 cm^{-1} band decreasing to 8% compared with 13% in the α-isoenzyme, and the 1619 cm^{-1} band fell to only 5%.

To better understand the effect of the different ligands on the thermal denaturation of the three domains and to compare these domains among themselves, the half-height widths of the FT-IR spectra of the amide I′ band were plotted against temperature (Figure 6), as it is known that these widths increase during protein denaturation (*41*). In the case of the spectra from the PKCα-C2 domain obtained in D_2O/EGTA buffer, major changes in the amide I′ mode were evident (Figure 6A) with a remarkable widening taking place between 40 and 55 °C. Denaturation (widening of the amide I′ band) occurred at the same temperature in the case of PKCβII-C2 (Figure 6B), although it is interesting that PKCγ-C2 was more resistant to heating, the widening only starting at 45 °C in this case (Figure 6C). The addition of 2 mM Ca^{2+} increased the temperature at which the onset of thermal denaturation occurred in PKCα-C2 from 40 to 60 °C (Figure 6A). In comparison, it can be observed that, in the presence of 2 mM Ca^{2+}, the denaturation onset occurred at only 50 °C for PKCβII-C2 (Figure 6B) and at 55 °C for PKCγ-C2 (Figure 6C). When the experiments were carried out in the presence of 12 mM $CaCl_2$, the whole process was shifted to higher temperatures for PKCα-C2 and PKCγ-C2, with the denaturation onset occurring at about 75 °C for both (Figure 6A and C), and 70 °C for PKCβII-C2 (Figure 6B), indicating that the domains had a higher stability when bound to Ca^{2+}, especially in the case of PKCα-C2 and PKCγ-C2. Finally, in the presence of 2 mM Ca^{2+} and PA/PC (4:1 molar ratio) vesicles, the onset of the widening process was also shifted to higher temperatures, being 70 °C for PKCα-C2 (Figure 6A), 65 °C for PKCβII-C2 (Figure 6B), and 75 °C for PKCγ-C2 (Figure 6C).

To gain further insight into the differences between the three C2 domains studied here, we carried out a 2D-IR analysis as a function of changes in temperature. The average spectrum of all the scans was used as reference for this analysis. Figure 7A shows the synchronous correlation contour map of PKCα-C2 in the presence of EGTA (absence of Ca^{2+}), when heated from 25 to 80 °C, at 5 °C intervals. This map shows two autopeaks at 1618 and 1636 cm^{-1}, indicating that the relative intensities of these bands changed with increasing temperature. The most intense cross-peaks were observed at these frequencies (1618−1636 cm^{-1}) and were negative, indicating, that during the heating process, one of them increased and the other one decreased. These observations can be more fully understood from the 1D studies described above: the disappearance of the β-sheet component associated with the appearance of the intermolecular β-sheet.

The synchronous spectrum from PKCβII-C2 in the presence of EGTA (Figure 7B) was similar to that of PKCα-C2. It showed two autopeaks: the first one is at 1619 cm^{-1}, and the second one has a very broad maximum peaking at 1637 cm^{-1}, indicating that the main changes in intensity related the aggregation with the β-sheet component. There was only one cross-peak, relating aggregation (1619 cm^{-1}) with β-sheet components (1637 cm^{-1}).

The synchronous spectrum contour map from PKCγ-C2 (Figure 7C) was also similar to those of the other two classical isoenzymes, showing two autopeaks at 1619−1636 cm^{-1} and a main cross-peak at 1619−1636 cm^{-1} of negative sign as in the other two isoenzymes.

The asynchronous correlation spectrum of PKCα-C2 (Figure 8A) showed several correlations, and we will comment on the main ones. There was an asynchronous cross-peak relating 1616 to 1636 cm^{-1}, which was positive, but since the corresponding synchronous correlation was negative, the change at 1616 cm^{-1}, that is, the appearance of aggregation, must have taken place after the change at 1636 cm^{-1}, corresponding to the disappearance of the β-sheet. The wavenumber 1616 cm^{-1} also appears to be correlated with 1673 cm^{-1}, showing an asynchronous negative cross-peak, and since the corresponding synchronous spectrum is positive, it may be deduced that the change at 1673 cm^{-1} occurred before the change at 1616 cm^{-1}. This correlation indicates that the disappearance of the antiparallel β-sheet precedes the appearance of the aggregated β-sheet.

Table 4: FT-IR Parameters of the Amide I′ Band Components of the Classical PKCα, βII, and γ C2 Domains in the Corresponding D_2O Buffers in the Presence of 2 mM Ca^{2+} and Small Unilamellar Vesicles Containing 20 mol % PC and 80 mol PA

	25 °C						80 °C					
	C2-PKCα domain		C2-PKCβII domain		C2-PKCγ domain		C2-PKCα domain		C2-PKCβII domain		C2-PKCγ domain	
assignment	position[a] (cm^{-1})	area[b] (%)	position (cm^{-1})	area (%)	position (cm^{-1})	area (%)	position (cm^{-1})	area (%)	position (cm^{-1})	area (%)	position (cm^{-1})	area (%)
β-turns	1690	3	1690	2	1690	3	1692	5	1691	4	1692	4
aggregated β-sheet							1679	13	1680	7	1679	8
antiparallel β-sheet	1676	7	1676	8	1676	7						
β-turns	1664	13	1663	14	1665	13	1666	18	1667	17	1667	18
α-helix	1655	18	1655	16	1656	17	1656	16	1657	14	1657	16
random	1644	23	1644	24	1645	24	1644	29	1644	36	1645	30
β-sheet	1633	36	1632	36	1631	36	1631	13	1631	11	1631	19
aggregated β-sheet							1618	6	1619	11	1619	5

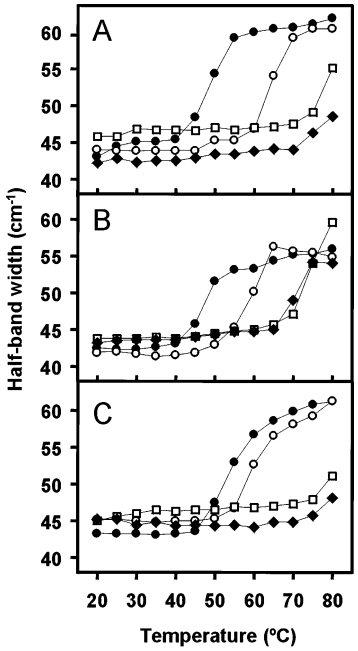

FIGURE 6: Half-bandwidth of the amide I′ region of the FT-IR spectra in inverse centimeters, as a function of temperature, from 20 to 80 °C, for the PKCα (A), the PKCβII (B), and the PKCγ-C2 domains (C), in the presence of 0.2 mM EGTA (●), 2 mM Ca^{2+} (○), 12 mM Ca^{2+} (◆), and 2 mM Ca^{2+}/SUV (PC:PA, 1:4) (□).

The other important asynchronous correlation was between 1636 and 1673 cm^{-1}, with a positive cross-peak, but since the corresponding synchronous spectrum was negative, the conclusion is that the change at 1673 cm^{-1} occurred before the change at 1635 cm^{-1}, so that the antiparallel β-sheet (1673 cm^{-1}) changed before the β-sheet (1635 cm^{-1}) started to disappear.

It is interesting that the asynchronous spectra corresponding to the other two classical isoenzymes were clearly different. In the case of PKCβII-C2 (Figure 8B), it showed a butterfly pattern characteristic of a band shift (*53*) occurring toward 1619 cm^{-1}, as a consequence of the aggregation that accompanies denaturation. There were three main asynchronous correlations, the first one being an asynchronous negative cross-peak at 1619−1630 cm^{-1}, indicating that the change at 1630 cm^{-1} (β-sheet) preceded that at 1619 cm^{-1} (aggregation). There was also an asynchronous negative cross-peak at 1630−1643 cm^{-1}, indicating that the change at 1643 cm^{-1} (nonstructured conformations) occurred first. Finally, there was an asynchronous positive correlation cross-peak at 1617−1650 cm^{-1}; however, in this case, the corresponding synchronous correlation was negative, and so the change at 1650 cm^{-1} (α-helix) preceded that at 1617 cm^{-1}.

Again PKCγ-C2 showed a different behavior from the other two isoenzymes (Figure 8C). The most important correlations here were as follows: An asynchronous cross-peak at 1620−1633 cm^{-1}, which was negative. But since there was a negative correlation in the synchronous spectrum, the change at 1633 cm^{-1} (β-sheet) occurred first. An asynchronous negative cross-peak at 1634−1647 cm^{-1} meant that the change at 1647 cm^{-1} (random) occurred first, as in the β-isoenzyme. In addition, another less marked correlation linked 1635 to 1657 cm^{-1}, this being negative, so that changes in the α-helix (1657 cm^{-1}) preceded those in the β-sheet (1635 cm^{-1}).

DISCUSSION

These differing sensitivities of the isolated C2 domains of three classical isoenzymes, PKCα, PKCβII, and PKCγ, to Ca^{2+}, lipid, and thermal unfolding revealed that although the 3D structures are in principle similar, there are subtle differences between them which may be significant when trying to explain their known function specializations. Their secondary structures are similar both in the presence and in the absence of Ca^{2+}. But some differences emerge when Ca^{2+} is used to protect from thermal unfolding, with the γ-isoenzyme being the most protected and the β-isoenzyme the least, so that the β-isoenzyme needed a considerably higher Ca^{2+} concentration to prevent the appearance of the intermolecular β-sheet, which is a signal of denaturation. The presence of phospholipid together with Ca^{2+} produced some changes at 25 °C in all the isoenzymes, with a decrease in the β-sheet and an increase in the random structure and α-helix as if the presence of phospholipid could influence the secondary structure of these domains. In the presence of phospholipids plus Ca^{2+}, the γ-isoenzyme was better protected than the α- and β-isoenzymes.

The use of infrared 2D correlation spectroscopy provided further insight into the unfolding mechanisms followed by the domains and revealed some differences between them. For example, the synchronous correlation pointed to substantial changes occurring at 1617−1619 cm^{-1}, that is, an increase in aggregation of the denaturated protein, and this correlation was detected in the three isoenzymes.

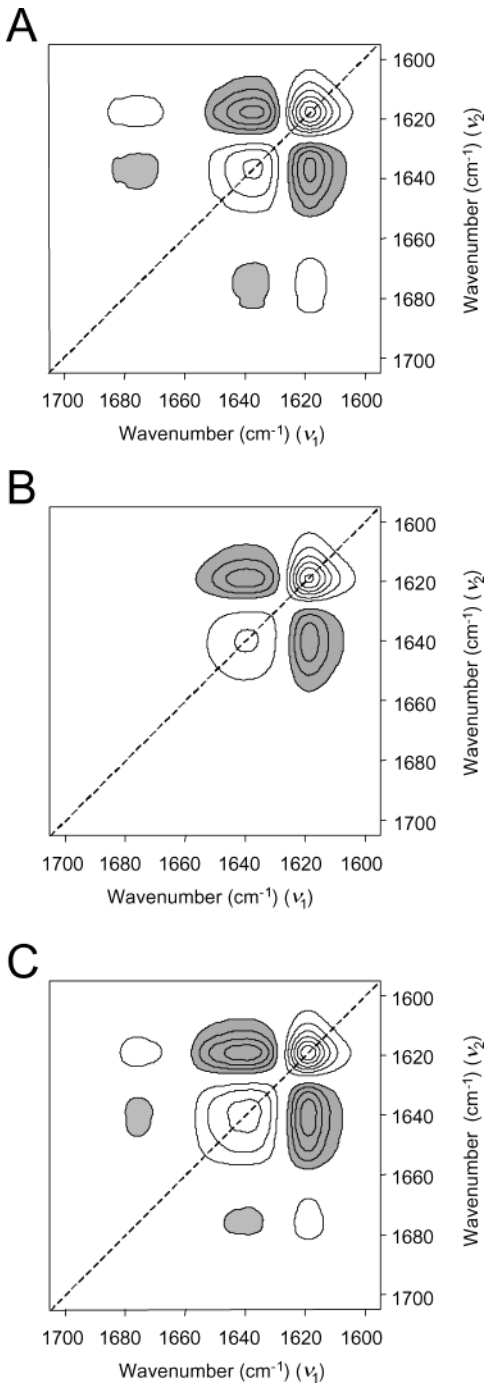

FIGURE 7: Synchronous 2D-IR correlation spectra of the PKCα (A), PKCβII (B), and PKCγ-C2 domains (C) as a function of temperature variation between 20 and 80 °C in the presence of 0.2 mM EGTA. The correlation spectra were obtained using the 2D-Pocha program. White and dark peaks are positive and negative correlations, respectively. The maximum correlation signals obtained were $3e^{-4}$, $8e^{-4}$, and $3e^{-4}$ for the PKCα, PKCβII, and PKCγ-C2 domains, respectively.

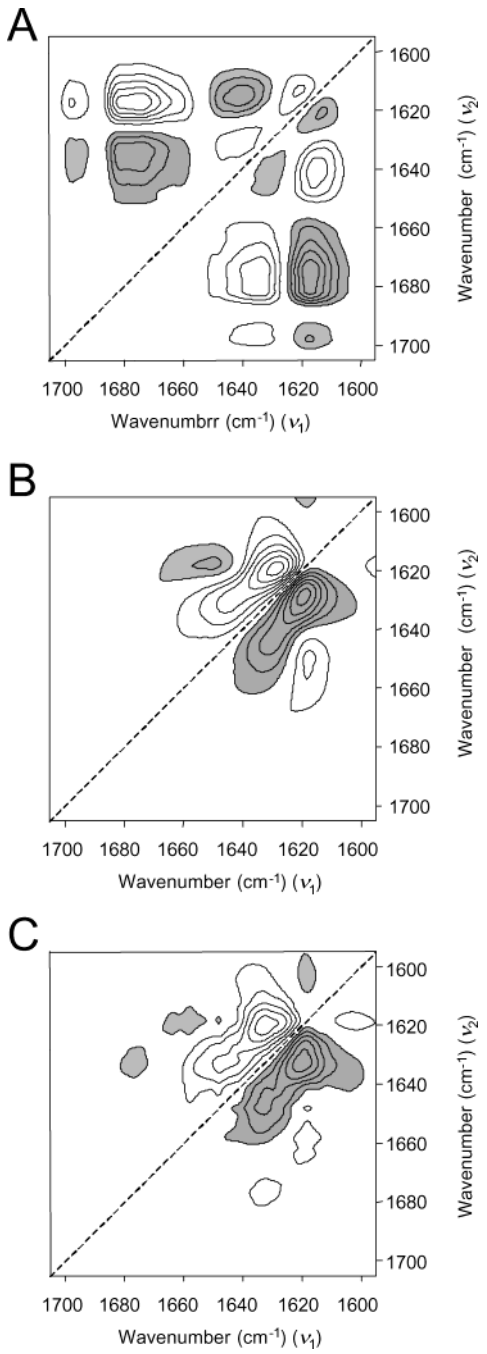

FIGURE 8: Asynchronous 2D-IR correlation spectra of the PKCα (A), PKCβII (B), and PKCγ-C2 domains (C) as a function of temperature variation between 20 and 80 °C in the presence of 0.2 mM EGTA. The correlation spectra were obtained using the 2D-Pocha program. White and dark peaks are positive and negative correlations, respectively. The maximum correlation signals obtained were $2e^{-5}$, $8e^{-5}$, and $3e^{-5}$ for the PKCα, PKCβII, and PKCγ-C2 domains, respectively.

On the other hand, the asynchronous 2D-IR correlation study of the domains in the absence of Ca^{2+} showed that in all cases the aggregation increased after changes in other structural components had occurred and that changes in antiparallel β-sheet (α-isoenzyme), α-helix (γ-isoenzyme), and random coil (β-isoenzyme and γ-isoenzyme) occurred before (at a lower temperature) changes in the β-pleated sheet. This may be better understood by looking at the structure of the C2 domain, in which the core of the protein is the β-sandwich that would be more resistant to thermal denaturation than other peripheral structures. It is nevertheless interesting that there are certain differences between the three domains, as indicated by the different correlations observed in each case. It is also worthy of comment that the butterfly pattern present in the β- and γ-isoenzymes is not so clear in the α-isoform, although in the last one a trace of this pattern is visible but the intensity is low, indicating that these correlations revealing band-shifting are much weaker in this case than in the other two. However, in this α-isoenzyme

Table 5: Comparison of the Secondary Structures of the C_2 Domains of PKCα and PKCβ Obtained from Different Techniques

	PKCα-C2 domain		PKCβ-C2 domain	
	3D[a]	FT-IR[b]	3D[c]	FT-IR[d]
β-sheet	54	59	59	57
α-helix	10	12	10	14
β-turns	21	18	17	17
random	15	11	14	12

[a] Reference 14. [b] This study, PKCα-C2 domain in the presence of 12 mM Ca^{2+} at 25 °C. [c] Reference 12. [d] This study, PKCβII-C2 domain in the presence of 12 mM Ca^{2+} at 25 °C.

there are very strong correlations, that is, clear differences in resistance to heating, in other components such as antiparallel β-sheet (1673 cm^{-1}) with respect to the β-pleated sheet (1636 cm^{-1}) and aggregated β-sheet (1616 cm^{-1}). Judging from both the asynchronous and synchronous correlations, it seems that the β-isoenzyme differs from the α-isoenzyme, with the γ-isoenzyme being more similar to the β-isoenzyme.

It should be stressed at this point that the different sensitivities of the three C2 domains studied here to thermal denaturation are likely to arise especially from different backbone motions and hence with dynamics more than with structure. This point has been investigated usually using other techniques such as ^{15}N-nuclear magnetic resonance spin−spin relaxation measurements (*54*) or disulfide trapping (*55*), but infrared spectroscopy may also yield information in this respect. It is important to underline this point, since the present infrared study gives insights into stability and dynamics that are not provided by earlier structural studies.

Since high-resolution structures of two of the isoforms studied here are known, it was found interesting to make a comparison with the results obtained through infrared spectroscopy in this work. Table 5 shows this comparison, and it can be seen that there is a reasonable agreement between both approaches. With respect to the PKCα-C2, the only significant difference concerns the estimation of the amount of β-sheet, that was 59% according to this work and 54% after X-ray diffraction studies (*14*). A smaller difference was found with respect to random coil with 11% in this work and 15% according to X-ray diffraction. A good agreement between both techniques was also found for the PKCβ-C2, with the only small discrepancy in the case of the α-helix, with 14% in this work and 10% after X-ray diffraction (*12*). The conclusion is then that infrared spectroscopy gives a reasonably good picture of the relative amounts of different secondary structures.

The specialization of the different cPKCs can be appreciated from their different roles with respect, for example, to cancer. PKCα overexpression leads to a more aggressive tumor phenotype (*56*), and phosphorothioate antisense directed at the AUG translation iniation codon of murine PKCα inhibits tumor growth in nude mice (*57*, *58*). On the other hand, it has been found that the elevated expression of PKCβI leads to the inhibition of growth in HT29 colon cancer cells and tumor suppression (*59*, *60*). PKCβI also causes loss of anchorage dependence, limits the growth to higher densities, and causes tumor formation of R6 rat fibroblasts in nude mice (*61*). It also blocks differentiation and increases proliferation (*62*, *63*). PKCβII, however, can be used as a marker for certain types of cancer, such as cancer of the colon. It has been observed, for example, that the level of PKCβII, but not of the other classical PKCs, dramatically increases in colonic hyperproliferation (*64*) and is selectively translocated to the nucleus of human promyelocytic (HL60) leukemia cells in vitro (*65*).

In addition, it has been reported that PKCα plays a role in cell−cell contact (*66*) and in the suppression of apoptosis (*67*). PKCβII increases in vascular cells exposed to high levels of glucose and seems to be involved in diabetes-induced vascular dysfunction (*68*) and diabetic retinopathy (*69*); its overexpression has also been implicated in heart failure and diabetic cardiovascular complications (*58*, *70*−*72*). On the other hand, PKCγ is expressed only in the central nervous system (*73*, *74*) and has been implicated in the development of injury-induced persistent pain (*75*, *76*). A rat PKCγ mutation has been described to cause a Parkinsonian syndrome (*77*), and a role for PKCγ in the control of lens cortical gap junctions has been suggested (*78*). Transgenic mouse knockouts have been established for PKCγ (*79*) and PKCβ (*80*) with associated mild neurological and immune disorders, respectively.

The differences found here between the domains suggest that these molecules have different abilities to adapt their 3D structures during the interaction with ligands, such as Ca^{2+} and phospholipids that play a key role in their activation.

Whereas the γ-isoenzyme is able to sense small increases in Ca^{2+}, much higher concentrations will be necessary to affect the structure of the β-isoenzyme. Docking of the full enzymes would depend primarily on the availability of Ca^{2+} to bridge the C2 domain to the membrane (*14*); it is therefore interesting to detect different sensitivities of the C2 domains to Ca^{2+} binding, since this may be an indication of differences in docking capacities. It is interesting, in this context, that the sensitivities observed here are very similar to those described by Kuhout et al. (*81*), who mentioned that a small Ca^{2+} transient would permit PKCγ to dock more efficiently than PKCα, which in turn would dock more effectively than PKCβ. These differences may be significant for the specialized functions of conventional PKC isoenzymes. As more information becomes available with respect to the individual roles in the cells of the different classical PKC isoenzymes, the contribution made by this work may be useful for better understanding their structure−function relationship.

ACKNOWLEDGMENT

We thank Drs. Ono and Nishizuka (Kobe, Japan) and Dr. T. Meyer (Stanford, CA) for the kind gifts of cDNAs. We also thank Drs. Adachi and Ozaki for making available his 2D-Pocha program for studying 2D-IR correlation spectroscopy.

REFERENCES

1. Mellor, H., and Parker, P. J. (1998) *Biochem. J. 332*, 281−292.
2. Hofmann, J. (1997) *FASEB J. 11*, 649−669.
3. Nishizuka, Y. (1995) *FASEB J. 9*, 484−496.
4. Sutton, R. B., Davletov, B. A., Berghuis, A. M., Südhof, T. C., and Sprang, S. R. (1995) *Cell 80*, 929−938.
5. Shao, X., Fernandez, I., Sudhof, T. C., and Rizo, J. (1998) *Biochemistry 37*, 16106−16115.
6. Sutton, R. B., Ernst, J. A., and Brunger, A. T. (1999) *J. Cell. Biol. 147*, 589−598.

7. Essen, L. O., Perisic, O., Cheung, R., Katan, M., and Williams, R. L. (1996) *Nature 380*, 595−602.
8. Grobler, J. A., Essen, L. O., Williams, R. L., and Hurley, J. H. (1996) *Nat. Struct. Biol. 3*, 788−795.
9. Perisic, O., Fong, S., Lynch, D. E., Bycroft, M., and Williams, R. L. (1998) *J. Biol. Chem. 273*, 1596−1604.
10. Xu, G. Y., McDonagh, T., Yu, H. A., Nalefski, E. A., Clark, J. D., and Cumming, D. A. (1998) *J. Mol. Biol. 280*, 485−500.
11. Dessen, A., Tang, J., Schmidt, H., Stahl, M., Clark, J. D., and Cumming, D. A. (1999) *Cell 97*, 349−360.
12. Sutton, R. B., and Sprang, S. R. (1998) *Structure 6*, 1395−1405.
13. Pappa, H., Murray-Rust, J., Dekker, L. V., Parker, P. J., and McDonald, N. Q. (1998) *Structure 6*, 885−894.
14. Verdaguer, N., Corbalán-García, S., Ochoa, W. F., Fita, I., and Gómez-Fernández, J. C. (1999) *EMBO J. 18*, 6329−6338.
15. Ochoa, W. F., Corbalán-García, S., Eritja, R., Rodríguez-Alfaro, J. A., Gómez-Fernández, J. C., Fita, I., and Verdaguer, N. (2002) *J. Mol. Biol. 320*, 277−291.
16. Ochoa, W. F., García-García, J., Fita, I., Corbalán-García, S., Verdaguer, N., and Gómez-Fernández, J. C. (2001) *J. Mol. Biol. 311*, 837−849.
17. Lee, J. O., Yang, H., Georgescu, M. M., Di Cristofano, A., Maehama, T., Shi, Y., Dixon, J. E., Pandolfi, P., and Pavletich, N. P. (1999) *Cell 99*, 323−334.
18. Walker, E. H., Perisic, O., Ried, C., Stephens, L., and Williams, R. L. (1999) *Nature 402*, 313−320.
19. Nalefski, E. A., and Falke, J. J. (1996) *Protein Sci. 5*, 2375−2390.
20. Rizo, J., and Südhof, T. C. (1998) *J. Biol. Chem. 273*, 15879−15882.
21. Bazzi, M. D., and Nelsestuen, G. L. (1990) *Biochemistry 29*, 7624−7630.
22. Luo, J. H., Kahn, S., O'Driscoll, K., and Weinstein, I. B. (1993) *J. Biol. Chem. 268*, 3715−3719.
23. Newton, A. C., and Keranen, L. M. (1994) *Biochemistry 33*, 6651−6658.
24. Edwards, A. S., and Newton, A. C. (1997) *Biochemistry 36*, 15615−15623.
25. Medkova, M., and Cho, W. (1998) *J. Biol. Chem. 273*, 17544−17552.
26. Ohno, S., Akita, Y., Hata, A., Osada, S., Kubo, K., Konno, Y., Akimoto, K., Mizuno, K., Saido, T., Kuroki, T., and Suzuki, K. (1991) *Adv. Enzyme Regul. 31*, 287−303.
27. Dempsey, E. C., Newton, A. C., Mochly-Rosen, D., Fields, A. P., Reyland, M. E., Insel, P. A., and Messing, R. O. (2000) *Am. J. Physiol.: Lung Cell. Mol. Physiol. 279*, L429−438.
28. Nishizuka, Y. (1992) *Science 258*, 607−614.
29. Coussens, L., Rhee, L., Parker, P. J., and Ullrich, A. (1987) *DNA 6*, 389−394.
30. Knopf, J. L., Lee, M. H., Sultzman, L. A., Kriz, R. W., Loomis, C. R., Hewick, R. M., and Bell, R. M. (1986) *Cell 46*, 491−502.
31. Ono, Y., Fujii, T., Igarashi, K., Kikkawa, U., Ogita, K., and Nishizuka, Y. (1988) *Nucleic Acids Res. 16*, 5199−5200.
32. Housey, G. M., Johnson, M. D., Hsiao, W. L., O'Brian, C. A., Murphy, J. P., Kirschmeier, P., and Weinstein, I. B. (1988) *Cell 52*, 343−354.
33. Arrondo, J. L. R., and Goñi, F. M. (1999) *Prog. Biophys. Mol. Biol. 72*, 367−405.
34. Noda, I. (1993) *Appl. Spectrosc. 47*, 1329−1336.
35. Noda, I., Dowerey, A. E., Marcott, C., Story, G. M., and Ozaki, Y. (2000) *Appl. Spectrosc. 54*, 236A−248A.
36. Ozaki, Y., Murayama, Wu Y., and Czarnik-Matusewicz, B. (2003) *Spectroscopy 17*, 79−100.
37. Garcia-Garcia, J., Corbalan-Garcia, S., and Gomez-Fernandez, J. C. (1999) *Biochemistry 38*, 9667−9675.
38. Smith, P. K., Krohn, R. I., Hermanson, G. T., Mallia, A. K., Gartner, F. H., Provenzano, M. D., Fujimoto, E. K., Goeke, N. M., Olson, B. J., and Klenk, D. C. (1985) *Anal. Biochem. 150*, 76−85.
39. Laemmli, U. K. (1970) *Nature 227*, 680−685.
40. Arrondo, J. L. R., Muga, A., Castresana, J., Bernabeu, C., and Goñi, F. M. (1989) *FEBS Lett. 252*, 118−120.
41. Arrondo, J. L. R., Castresana, J., Valpuesta, J. M., and Goñi, F. M. (1994) *Biochemistry 33*, 11650−11655.
42. Krimm, S., and Bandekar, J. (1986) *Adv. Protein Chem. 38*, 181−364.
43. Susi, H., and Byler, D. M. (1987) *Arch. Biochem. Biophys. 258*, 465−469.
44. Fabian, H., Naumann, D., Misselwitz, R., Ristau, O., Gerlach, D., and Welfle, H. (1992) *Biochemistry 31*, 6532−6538.
45. Gonzalez, M., Bagatolli, L. A., Echabe, I., Arrondo, J. L. R., Argaraña, C. E., Cantor, C. R., and Fidelio, G. D. (1997) *J. Biol. Chem. 272*, 11288−11294.
46. Zhang, H., Ishikawa, Y., Yamamoto, Y., and Carpentier, R. (1998) *FEBS Lett. 426*, 347−351.
47. Muga, A., Arrondo, J. L. R., Bellon, T., Sancho, J., and Bernabeu, C. (1993) *Arch. Biochem. Biophys. 300*, 451−455.
48. Bandekar, J. (1992) *Biochim. Biophys. Acta 1120*, 123−143.
49. Susi, H., Timasheff, S. N., and Stevens, L. (1967) *J. Biol. Chem. 242*, 5460−5466.
50. Cladera, J., Galisteo, M. L., Sabes, M., Mateo, P. L., and Padros, E. (1992) *Eur. J. Biochem. 207*, 581−585.
51. Surewicz, W. K., Leddy, J. J., and Mantsch, H. H. (1990) *Biochemistry 29*, 8106−8111.
52. Susi, H. (1972) *Methods Enzymol. 26*, 455−472.
53. Arrondo, J. L. R., Iloro, I., Aguirre, J., and Goñi, F. M. (2003) *Spectroscopy* (in press).
54. Johansson, M. U., Nilsson, H., Evenas, J., Forsen, S., Drakenberg, T., Bjorrck, L., and Wikstrom, M. (2002) *J. Mol. Biol. 316*, 1083−1099.
55. Careaga, C. L., and Falke, J. J. (1992) *J. Mol. Biol. 226*, 1219−1225.
56. Ways, D. K., Kukoly, C. A., de Vente, J., Hooker, J. L., Bryant, W. O., Posekany, K. J., Fletcher, D. J., Cook, P. P., and Parker, P. J. (1995) *J. Clin. Invest. 95*, 1906−1915.
57. Yazaki, T., Ahmad, S., Chahlavi, A., Zylber-Katz, E., Dean, N. M., Rabkin, S. D., Martuza, R. L., and Glazer, R. I. (1996) *Mol. Pharmacol. 50*, 236−242.
58. Dean, N., McKay, R., Miraglia, I., Howard, R., Cooper, S., Giddings, J., Nicklin, P., Meister, L., Ziel, R., Geiger, T., Muller, M., and Fabbro, D. (1996) *Cancer Res. 56*, 3499−3507.
59. Goldstein, D. R., Cacace, A. M., and Weinstein, I. B. (1995) *Carcinogenesis 16*, 1121−1126.
60. Choi, P. M., Tchou-Wong, K. M., and Weinstein, I. B. (1990) *Mol. Cell Biol. 10*, 4650−4657.
61. Borner, C., Ueffing, M., Jaken, S., Parker, P. J., and Weinstein, I. B. (1995) *J. Biol. Chem. 270*, 78−86.
62. Sauma, S., Yan, Z., Ohno, S., and Friedman, E. (1996) *Cell Growth Differ. 7*, 587−594.
63. Khuri, F. R., Cho, Y., and Talmage, D. A. (1996) *Cell Growth Differ. 7*, 595−602.
64. Murray, N. R., Davidson, L. A., Chapkin, R. S., Clay Gustafson, W., Schattenberg, D. G., and Fields, A. P. (1999) *J. Cell Biol. 145*, 699−711.
65. Hocevar, B. A., and Fields, A. P. (1991) *J. Biol. Chem. 266*, 28−33.
66. Llosas, M. D., Batlle, E., Coll, O., Skoudy, A., Fabre, M., and Garcia de Herreros, A. (1996) *Biochem. J. 315*, 1049−1054.
67. Romanova, L. Y., Alexandrov, I. A., Schwab, G., Hilbert, D. M., Mushinski, J. F., and Nordan, R. P. (1996) *Biochemistry 35*, 9900−9906.
68. Inoguchi, T., Battan, R., Handler, E., Sportsman, J. R., Heath, W., and King, G. L. (1992) *Proc. Natl. Acad. Sci. U.S.A. 89*, 11059−63.
69. Frank, R. N. (2002) *Am. J. Ophthalmol. 133*, 693−698.
70. Cornford, P., Evans, J., Dodson, A., Parsons, K., Woolfenden, A., Neoptolemos, J., and Foster, C. S. (1999) *Am. J. Pathol. 154*, 137−144.
71. Bowling, N., Walsh, R. A., Song, G., Estridge, T., Sandusky, G. E., Fouts, R. L., Mintze, K., Pickard, T., Roden, R., Bristow, M. R., Sabbah, H. N., Mizrahi, J. L., Gromo, G., King, G. L., and Vlahos, C. J. (1999) *Circulation 99*, 384−391.
72. Wakasaki, H., Koya, D., Schoen, F. J., Jirousek, M. R., Ways, D. K., Hoit, B. D., Walsh, R. A., and King, G. L. (1997) *Proc. Natl. Acad. Sci. U.S.A. 94*, 9320−9325.
73. Nishizuka, Y. (1988) *Nature 334*, 661−665.
74. Bell, R. M., and Burns, D. J. (1991) *J. Biol. Chem. 266*, 4661−4664.
75. Basbaum, A. I. (1999) *Proc. Natl. Acad. Sci. U.S.A. 96*, 7739−7743.
76. Martin, W. J., Malmberg, A. B., and Basbaum, A. I. (2001) *J. Neurosci. 21*, 5321−5327.
77. Craig, N. J., Duran Alonso, M. B., Hawker, K. L., Shiels, P., Glencorse, T. A., Campbell, J. M., Bennett, N. K., Canham, M., Donald, D., Gardiner, M., Gilmore, D. P., MacDonald, R. J.,

Maitland, K., McCallion, A. S., Russell, D., Payne, A. P., Sutcliffe, R. G., and Davies, R. W. (2001) *Nat. Neurosci. 4*, 1061−1062.

78. Saleh, S. M., Takemoto, L. J., Zoukhri, D., and Takemoto, D. J. (2001) *Mol. Vision 7*, 240−246.
79. Abeliovich, A., Paylor, R., Chen, C., Kim, J. J., Wehner, J. M., and Tonegawa, S. (1993) *Cell 75*, 1263−1271.
80. Leitges, M., Schmedt, C., Guinamard, R., Davoust, J., Schaal, S., Stabel, S., and Tarakhovsky, A. (1996) *Science 273*, 788−791.
81. Kohout, S. C., Corbalan-Garcia, S., Torrecillas, A., Gomez-Fernandez, J. C., and Falke, J. J. (2002) *Biochemistry 41*, 11411−11424.

BI034759+